Does a crouched leg posture enhance running stability and robustness?

Yvonne Blum, Aleksandra Birn-Jeffery, Monica A. Daley, Andre Seyfarth

www.elsevier.com/locate/yjtbi

Does a crouched leg posture enhance running stability and robustness?

Yvonne Blum, Aleksandra Birn-Jeffery, Monica A. Daley, Andre Seyfarth

PII: S0022-5193(11)00230-X
DOI: doi:10.1016/j.jtbi.2011.04.029
Reference: YJTBI6460

To appear in: *Journal of Theoretical Biology*

Received date: 13 August 2010
Revised date: 23 April 2011
Accepted date: 27 April 2011

Cite this article as: Yvonne Blum, Aleksandra Birn-Jeffery, Monica A. Daley and Andre Seyfarth, Does a crouched leg posture enhance running stability and robustness?, *Journal of Theoretical Biology*, doi:10.1016/j.jtbi.2011.04.029

Does A Crouched Leg Posture Enhance Running Stability and Robustness?

Yvonne Blum[a,*], Aleksandra Birn-Jeffery[b], Monica A. Daley[b], Andre Seyfarth[a]

[a] *Lauflabor Locomotion Laboratory, University of Jena, Dornburger Str. 23, 07743 Jena, Germany*

[b] *Structure and Motion Laboratory, Royal Veterinary College, Hawkshead Lane, Hatfield, Hertfordshire, UK*

Abstract

Humans and birds both walk and run bipedally on compliant legs. However, differences in leg architecture may result in species-specific leg control strategies as indicated by the observed gait patterns. In this work, control strategies for stable running are derived based on a conceptual model and compared with experimental data on running humans and pheasants (*Phasianus colchicus*). From a model perspective, running with compliant legs can be represented by the planar spring mass model and stabilized by applying swing leg control. Here, linear adaptations of the swing leg parameters, leg angle, leg length and leg stiffness, are assumed. Experimentally observed kinematic control parameters (leg rotation and leg length change) of human and avian running are compared, and interpreted within the context of this model, with specific focus on stability and robustness characteristics. The results suggest differences in stability characteristics and applied control strategies of human and avian running, which may relate to differences in leg posture (straight leg posture in humans, and crouched leg posture in birds). It has been suggested that crouched leg postures may improve stability. However, as the system of control strategies is overdetermined, our model findings suggest that a crouched leg posture does not necessarily enhance running stability. The model also predicts different leg stiffness adaptation rates for human and avian running, and suggests that a crouched avian leg

*Corresponding author. Tel: +49-3641-945729, Fax: +49-3641-945732
Email address: Yvonne.Blum@uni-jena.de (Yvonne Blum)

posture, which is capable of both leg shortening and lengthening, allows for stable running without adjusting leg stiffness. In contrast, in straight-legged human running, the preparation of the ground contact seems to be more critical, requiring leg stiffness adjustment to remain stable. Finally, analysis of a simple robustness measure, the normalized maximum drop, suggests that the crouched leg posture may provide greater robustness to changes in terrain height.

Keywords: Spring mass model (SLIP), Leg parameter adaptation, Human and avian locomotion

---

List of symbols, terms and definitions

Nomenclature

CoM	center of mass
CoP	center of pressure
GRF	ground reaction force
GSM	ground speed matching
TD	touch down
TDc	touch down of the contralateral leg
TO	take off
TOc	take off of the contralateral leg

Dimensional variables

α_{TD}	angle of attack [deg]
$\dot{\alpha}$	changing rate of the leg angle [deg/T]
BW	body weight [N]
Δh_{max}	maximum drop [m]
ΔL	leg compression [m]
E	system energy [J]
F_{max}	maximum leg force [BW]
g	gravitational acceleration [m/s^2]
γ	angle of approach [deg]
k_{Leg}	leg stiffness [BW/L_0]
k_{TD}	spring stiffness at TD [BW/L_0]
$\dot{k}$	changing rate of the leg stiffness [k_{TD}/T]
L_0	resting leg length [m]
$\dot{L}$	changing rate of the leg length [L_0/T]
m	body mass [kg]
NMD	normalized maximum drop [L_0]
t_{C}	contact time [s]
t_{F}	flight time [s]
t_{Fall}	falling time from apex to TD [s]
T	gait cycle [s]
v_{x}	horizontal component of the CoM velocity [m/s]
v_{y}	vertical component of the CoM velocity [m/s]
$v_{\mathrm{x,Ref}}$	reference speed [m/s]
y_{A}	apex height [m]
$y_{\mathrm{i}}, y_{\mathrm{i+1}}$	apex heights of two subsequent apices [m]

Non-dimensional variables

$$\mathrm{DF} = \frac{t_{\mathrm{C}}}{2\,(t_{\mathrm{C}} + t_{\mathrm{F}})} \qquad \text{duty factor}$$

$$\mathrm{Fr} = \frac{v_{\mathrm{x}}^2}{g\,L_0} \qquad \text{Froude number}$$

1. Introduction

The great majority of living terrestrial vertebrates are quadrupeds. However, bipedalism can be found within a few families of mammals, reptiles and within all birds. Among mammals, various groups of primates (Schmitt, 2003), the macropods (Windsor and Dagg, 2010) and a few groups of heteromyd rodents (Djawdan, 1993) locomote bipedally. Within reptiles, some families of lizards are also capable of bipedal locomotion (Aerts et al., 2003), especially when running at high speeds (Irschick and Jayne, 1999). While macropods, some smaller birds and heteromyd rodents move by hopping on both legs simultaneously, primates, lizards and larger birds use striding gaits. In this paper, we concentrate on bipedal running and compare two types of leg architecture: The straight leg posture, represented by the human leg, and the crouched leg posture, represented by the avian leg. Associated with these differences in leg architecture, the movement strategies of these two species differ fundamentally from each other. While humans are plantigrade, birds are digitigrade, whereby their elongated tarsometatarsals keep their ankles clearly off the ground during walking and running (Alexander, 2004). This avian leg geometry in combination with the crouched leg posture allows for leg lengthening before touching the ground and thereby coping with large ground disturbances, as it was impressively demonstrated by experiments on running guinea fowl (*Numida meleagris*) (Daley et al., 2006, 2007).

In general, legged locomotion can be described by spring-like leg behavior (Alexander, 2002) and here, the leg function is represented by the planar spring mass model, which is a well-established template to describe running (Blickhan, 1989; McMahon and Cheng, 1990) and walking (Geyer et al., 2006). For adequate leg parameter adjustments (angle of attack, leg stiffness and leg length) and sufficient speeds (e.g. $v_x > 3\,\mathrm{m/s}$ for human-like dimensions), the spring mass model shows self-stabilizing behavior (Seyfarth et al., 2002). However, periodic running solutions that are unstable without control can also be stabilized. It has been shown that swing leg retraction is one elegant approach to enhance stability in locomotion for both quadrupedal galloping (Herr and McMahon, 2001) and bipedal running (Seyfarth et al., 2003). This control strategy, namely the adaptation of the leg angle during the swing phase, can be extended to all three leg parameters: leg angle, leg length and leg stiffness (Blum et al., 2010).

This work investigates human and avian running by assuming such a swing leg control strategy, namely the linear adaptation of the three leg

parameters during late swing phase, in anticipation of the ground contact. Previous work observed adaptation of the foot's landing velocity to running speed (De Wit et al., 2000), indicating a speed-dependent leg retraction and leg length change in preparation for ground contact. The adaptation of the leg stiffness during swing phase was suggested in a recent study on running on uneven ground (Grimmer et al., 2008). Furthermore, experiments on running birds have demonstrated that retraction and lengthening of the leg during swing phase prevent the birds from falling (Daley et al., 2007).

Stability is the system's ability to reduce a deviation in the center of mass trajectory caused by a onetime perturbation. To evaluate the stability of a running pattern, limit cycle stability analysis (Dingwell and Kang, 2007; McGeer, 1993) is used. The robustness, in terms of the maximum perturbation the system can cope with, can be determined by estimating the size of the basin of attraction (Rummel et al., 2010). However, this analysis requires the assumptions that (i) the system is energy conserving and (ii) returns to the same limit cycle trajectory after the perturbation. This makes the analysis difficult to compare to experimental data on which those assumption might be violated. As an alternative, the normalized maximum drop (NMD) is calculated, which defines the maximum perturbation before stance is missed completely (Daley and Usherwood, 2010). This boundary condition measure is intuitive and easy to calculate, can be compared to experimental data, and makes no explicit assumptions about how the system deals with the energy associated with the perturbation.

The purpose of this work is to evaluate the stability and robustness characteristics of running with a straight versus a crouched leg posture, using both experimental data and predictions of the spring mass model. Previous experimental observations on human and avian running suggest that birds, compared to humans, are able to negotiate much larger perturbations when running on uneven terrain. Therefore, we hypothesize that the crouched leg posture of the avian leg provide greater running stability and robustness than the straight leg posture of humans.

2. Methods

2.1. Model

The simplest template to describe the dynamics of bouncing gaits like human and avian running is the planar spring mass model (Blickhan, 1989; McMahon and Cheng, 1990). In this model, the center of mass (CoM) is

represented by a point mass m, which is supported by a linear spring representing the leg. Assuming that the system is energy conserving, the system is fully described by three leg parameters at the instant of touch down (TD): angle of attack α_{TD}, leg stiffness k_{TD} and resting length of the leg spring L_0. The CoM undergoes alternating flight and stance phases, with the transition from flight to stance occurring when the landing condition $y = L_0 \sin\alpha_{\mathrm{TD}}$ is fulfilled. Since the system is conservative and with the assumption that the ground is even, the system's state is fully described by the apex condition $(y_{\mathrm{A}}, v_{\mathrm{x}})$. The apex is the highest point of the CoM-trajectory with zero vertical velocity. Therefore, the system energy

$$E = \frac{1}{2} m v_{\mathrm{x}}^2 + m g y_{\mathrm{A}} \tag{1}$$

is determined by the horizontal velocity v_{x} and the apex height y_{A}. To give this energy a more intuitive meaning, we define the reference speed

$$v_{\mathrm{x,Ref}} = \sqrt{2\left(\frac{E}{m} - g L_0\right)}, \tag{2}$$

assuming that the apex height y_{A} equals the resting leg length L_0.

The spring mass model is capable of running with fixed landing conditions: for adequate leg parameters and sufficiently high running speeds, the system shows self-stabilizing behavior (Seyfarth et al., 2002). However, by adjusting the leg parameters during swing phase (e.g. swing leg retraction (Seyfarth et al., 2003)), it is possible to stabilize running patterns which are unstable without control. Here we assume linear adaptations of the leg parameters (Blum et al., 2010)

$$\begin{aligned} \alpha(t) &= \alpha_{\mathrm{A}} + \dot{\alpha}\,(t - t_{\mathrm{A}}) \\ k(t) &= k_{\mathrm{A}} + \dot{k}\,(t - t_{\mathrm{A}}) \\ L(t) &= L_{\mathrm{A}} + \dot{L}\,(t - t_{\mathrm{A}}), \end{aligned} \tag{3}$$

beginning at the instant of apex t_{A} and continuing during the second half of the flight phase (figure 1). The apex conditions α_{A}, k_{A} and L_{A} are calculated such that, if the system is not disturbed, the landing conditions α_{TD}, k_{TD} and L_{TD} remain the same for every parameter adaptation rate $\dot{\alpha}$, $\dot{k}$ and $\dot{L}$.

To characterize the running patterns, we analyze the direction and the magnitude of the foot landing velocity (Blum et al., 2010). Although the leg

of the spring mass model is massless, this analysis approximates the size of the impact a real leg would experience. With increasing landing velocity of the foot, the landing impact would increase as well. The relative speed of the foot point defines the *ground speed matching* (GSM)

$$\mathrm{GSM} = 1 - \frac{v_{\mathrm{Foot}}}{v_{\mathrm{CoM}}}, \tag{4}$$

where v_{Foot} is the speed of the foot point and v_{CoM} the speed of the CoM at TD. The foot's landing direction defines the *angle of approach*

$$\gamma = \tan^{-1}\left(\frac{v_{\mathrm{x,Foot}}}{v_{\mathrm{y,Foot}}}\right) + 180^{\circ}, \tag{5}$$

which is the angle between the foot velocity vector $\mathbf{v}_{\mathrm{Foot}}$ and the ground (figure 2).

2.2. Stability analysis

We estimate the stability of a running pattern based on the spring mass model. The vertical movement of the CoM describes an oscillation, which can be analyzed using a Poincaré map. We define the Poincaré section at the instant of apex and therefore, the corresponding map $y_{\mathrm{i+1}}(y_{\mathrm{i}})$ is the apex-return map of two subsequent apices y_{i} and $y_{\mathrm{i+1}}$ (figure 3). In this Poincaré map, periodic running solutions (also known as limit cycle trajectories (Dingwell and Kang, 2007; McGeer, 1993)) are identified by fixed points y^*, which satisfy (i) the identity $y_{\mathrm{i}} = y_{\mathrm{i+1}}$, while (ii) maintaining positive horizontal velocity $v_{\mathrm{x,i}} = v_{\mathrm{x,i+1}} > 0$. The stability of such a periodic running solution is estimated by analyzing the slope s of the apex-return map $y_{\mathrm{i+1}}(y_{\mathrm{i}})$ in the neighborhood of the fixed point y^* (Geyer et al., 2005) (Appendix A). If the absolute value of the derivative

$$s = \left.\frac{dy_{\mathrm{i+1}}}{dy_{\mathrm{i}}}\right|_{y^*} \tag{6}$$

is smaller than one ($|s| < 1$), the fixed point and therefore the corresponding periodic running pattern is stable (Strogatz, 1994).

2.3. Gait robustness

The robustness of a stable running solution is defined as the maximum perturbation the system can cope with, and its upper bound can be approximated by the *normalized maximum drop* (NMD)

$$\mathrm{NMD} = \frac{\Delta h_{\mathrm{max}}}{L_0}, \tag{7}$$

which defines the maximum perturbation before stance is missed completely (Daley and Usherwood, 2010). The extended NMD (hereinafter referred to as NMD) indicates the maximum drop $\Delta h_{\max}$ relative to the leg length L_0, the runner could negotiate, assuming (i) the leg continues retracting with constant leg retraction speed, (ii) the leg length continues lengthening or shortening with constant changing rate, and (iii) $\Delta h_{\max}$ is reached when the leg is vertically oriented ($\alpha = 90°$). Under these assumptions, $\Delta h_{\max}$ is a function of the kinematic parameters angle of attack α_{TD}, leg retraction speed $\dot{\alpha}$ and leg length change $\dot{L}$ (Appendix B).

2.4. Experiments

Experimental data on human running were collected by Lipfert (2010). Seven human subjects (one female, six males, body mass $m = 77 \pm 9\,\mathrm{kg}$, leg length $L_0 = 1.02 \pm 0.07\,\mathrm{m}$) were running on an instrumented treadmill at three different speeds, namely 2 m/s (Fr = 0.42), 3 m/s (Fr = 0.94) and 4 m/s (Fr = 1.66) and a total of 2867 running gait cycles were analyzed. The initial vertical position of the CoM, which corresponds to the leg's rest length L_0, was approximated by the vertical position of the greater trochanter multiplied with a gender specific factor A ($A = 1.05$ for women and $A = 1.10$ for men) (Lipfert, 2010). CoM movements were calculated by twice integrating the accelerations obtained from the ground reaction forces (GRF) and the effective leg was defined as the distance between CoM and center of pressure (CoP). The horizontal velocity v_{x} of the CoM was determined at the instant of apex. The contact time t_{C} was measured from TD to take off (TO), the flight time t_{F} was calculated by subtracting contact time from step time (half of the gait cycle T). To determine the leg angle during flight, a hybrid leg was defined between the foot point (located half way between heel and toe) and the CoM, and the leg angle was measured with respect to the horizontal, which increases with leg retraction. The time derivatives of the experimentally observable leg parameters ($\dot{\alpha}$, $\ddot{\alpha}$, $\dot{L}$ and $\ddot{L}$) were estimated at the instant before TD.

Avian running trials were conducted on a $0.6 \times 4.5\,\mathrm{m}$ runway. Five $0.6 \times 0.9\,\mathrm{m}$ force plates (model 9287B, Kistler, Winterthur, Switzerland) were arranged in a row to record the GRF, and a camera system (Qualisys, Gothenburg, Sweden), consisting of eight high speed infrared cameras, was used to capture body kinematics. To approximate the CoM position and the foot point, two markers were attached to the birds' back (cranial and caudal), one at digit III and one at the tarsometatarsophalangeal joint. Five

male pheasants (*Phasianus colchicus*, body mass $m = 1.2 \pm 0.1\,\mathrm{kg}$, standing hip height $L_0 = 0.21 \pm 0.01\,\mathrm{m}$) were encouraged to run from one end of the runway to the other, and a total of 62 running steps at speeds between $\mathrm{Fr} = 2.32$ and $\mathrm{Fr} = 3.68$ were analyzed. Since we could not control the birds' running speeds, we analyzed the speed in post-processing. The horizontal velocity v_x of the CoM was determined at the instant of apex and the corresponding steps were divided into Froude number categories of $\mathrm{Fr} = 2$, 3 and 4 (meaning, for instance, that Froude numbers within the interval $\mathrm{Fr} = [1.5, 2.5)$ are assigned to category $\mathrm{Fr} = 2$). The initial vertical position of the CoM was defined by the average of the cranial and caudal marker position, and the initial velocity condition was estimated corresponding to Daley et al. (2006). CoM movements, contact time t_C, flight time t_F and time derivatives of the leg parameters were estimated as mentioned above, with the hybrid leg being defined between foot point (located half way between digit III and tarsometatarsophalangeal joint) and CoM.

Human running data were measured on a treadmill, while avian data were collected using an overground runway. The comparison of treadmill and overground running can be somewhat problematic, as joint angle kinematics may differ slightly, even though the cause of these discrepancies is not completely understood (Nelson et al., 1972; Nigg et al., 1995). Nonetheless, as long as the speed of the treadmill belt is constant, and dynamics and kinematics are not measured during belt acceleration, there exists no fundamental mechanical difference between treadmill and overground running (Van Ingen Schenau, 1980). Therefore, for the purposes of our comparison to the spring mass model, this difference between the two datasets is unlikely to substantially alter the findings.

The stiffness of a leg spring, assuming a linear force-length relationship, is defined as $k_{\mathrm{Leg}} = \frac{F_{\max}}{\Delta L}$, with $F_{\max}$ being the maximum value of the GRF and ΔL the maximum leg compression during stance. Assuming an elastic leg function, the GRF can be approximated by a sine function (Alexander, 1989; Dalleau et al., 2004). With this, k_{Leg} reduces to a function of body mass m, resting leg length L_0, duty factor DF and angle of attack α_{TD} (Blum et al., 2009; Morin et al., 2005).

To estimate the stability of spring mass running, periodic solutions (section 2.2) have to be found based on experimental data. Within the spring mass model, a periodic solution is uniquely determined by four parameters (Energy E, angle of attack α_{TD}, leg stiffness k_{TD} and leg length L_0 (section 2.1)). However, the angle of attack α_{TD} is the parameter that matches the

least with the model. On the one hand, the CoP is shifted during stance due to the roll-over characteristic of the foot (Bullimore and Burn, 2006), and on the other hand, the human leg angles at TD and TO are asymmetric with respect to the vertical axis (Cavagna, 2006). Both effects are not considered in the simple spring mass model. Therefore, to estimate periodic solutions, symmetric angles of attack $\alpha_{\mathrm{TD,sym}}$ were estimated based on the observed flight time after apex (falling time t_{fall}), assuming simulated contact phases, which are symmetric with respect to the vertical axis (Blum et al., 2010).

2.5. Data analysis and simulation

Experimental data analysis and numerical calculations were implemented in Matlab (version R2007b, The MathWorks™, Natick, MA, USA), the spring mass model in Matlab/Simulink. For numerical integration a built-in variable timestep integrator (ode113) was used with an absolute and relative error tolerance of 10^{-9}.

3. Results

The comparison of human (table 1) and avian (table 2) leg parameters reveals some fundamental differences in running strategies and applied control strategies (table 3 and figure 4). Compared to birds, humans touch the ground with steeper angles of attack α_{TD}, which decrease with increasing running speed. By contrast, the avian angles of attack do not change significantly. While in human running the leg's angular acceleration $\ddot{\alpha}$ increases with increasing running speed, the avian $\ddot{\alpha}$ shows no significant trend. However, the most conspicuous difference is that humans shorten their legs before TD ($\dot{L} < 0$), while birds lengthen them ($\dot{L} > 0$). With increasing running speed the human leg shortening enhances slightly, whereas the avian leg lengthening does not change significantly. While the avian leg length acceleration $\ddot{L}$ increases with increasing running speed, the human $\ddot{L}$ decreases. Compared to birds, humans touch the ground with a flatter angle of approach ($\gamma > 150°$ for humans, $\gamma < 150°$ for birds). Furthermore, with increasing running speed the human angle of approach γ gets flatter, whereas the avian γ does not change significantly.

Despite all differences, there also exist some similar tendencies in leg parameter adaptation for both humans and birds. For both, the angular velocity $\dot{\alpha}$ increases with increasing running speed. Although, compared to birds, humans run with stiffer legs, for both the leg stiffness k_{TD} does

not change significantly with speed. For low speeds the model predicts the lowest stiffness adaptation rate $\dot{k}$ for the mean value of the kinematic control strategies ($\dot{k} = -1.6k_{\mathrm{TD}}/T$ at $\mathrm{Fr} = 0.42$ for humans, $\dot{k} = -0.2k_{\mathrm{TD}}/T$ at $\mathrm{Fr} = 2.36$) and with increasing speed $\dot{k}$ increases as well. However, humans might exploit a much bigger range of stiffness adaptation rates than birds ($\Delta\,\mathrm{Fr} = 1.24$ and $\Delta\dot{k} = 3.2k_{\mathrm{TD}}/T$ for humans, $\Delta\,\mathrm{Fr} = 1.27$ and $\Delta\dot{k} = 0.7k_{\mathrm{TD}}/T$ for birds). For both humans and birds the GSM increases and the NMD decreases with increasing running speed.

Figure 5 shows the kinematic leg parameters, leg angle $\alpha(t)$ and leg length $L(t)$, for human (subfigures (a) and (b)) and avian (subfigures (c) and (d)) running mapped against each other. One orbit describes one stride cycle, beginning and ending with the TD of the same leg. For the averaged trajectories (indicated by the green, respectively red lines), the instants of TD and TO of the ipsi- and the contralateral leg are displayed. As the graphs contain no direct time information, it should be noted that the durations of the stance phases of the ipsilateral and the contralateral leg (i.e. the elapsing time between TD and TO, respectively TDc and TOc) within each graph are similar, as we were investigating symmetric running. Humans touch and leave the ground with a leg length that is comparable to the resting leg length L_0 of the hybrid leg (section 2.4) ($L_{\mathrm{TD}} = 1.01 \pm 0.01L_0$ and $L_{\mathrm{TO}} = 0.99 \pm 0.06L_0$ for $\mathrm{Fr} = 0.42$, $L_{\mathrm{TD}} = 1.01 \pm 0.01L_0$ and $L_{\mathrm{TO}} = 1.00 \pm 0.06L_0$ for $\mathrm{Fr} = 1.66$). Their phase plots are asymmetric (section 2.4: asymmetry of the human stance phase), whereas the avian phase plots are more symmetrical with respect to the leg angle in both phases stance and swing, and can be mirrored at $\alpha = 90°$. Compared to the resting leg length L_0, which is defined as the standing hip height, birds touch and leave the ground with more extended legs ($L_{\mathrm{TD}} = 1.25 \pm 0.04L_0$ and $L_{\mathrm{TO}} = 1.18 \pm 0.06L_0$ for $\mathrm{Fr} = 2.32$, $L_{\mathrm{TD}} = 1.23 \pm 0.05L_0$ and $L_{\mathrm{TO}} = 1.18 \pm 0.04L_0$ for $\mathrm{Fr} = 3.68$). Even during the entire stance phase, the avian leg does not compress below L_0.

In figure 6, control strategies ($\dot{\alpha}$, $\dot{k}$ and $\dot{L}$) leading to stable spring mass running are shown for four different periodic solutions (subfigures (a) and (b) for human, (c) and (d) for avian parameters) and compared with experimental data. The illustrated space is spanned by the kinematic control parameters $\dot{\alpha}$ and $\dot{L}$. Depending on these kinematic control parameters, the ground speed matching (GSM) and the angle of approach γ are calculated, and selected isolines of GSM and γ are mapped within the ($\dot{\alpha}$,$\dot{L}$)-space. The gray wedges indicate stable areas with $|s| < 0.5$ that correspond to the displayed stiffness adaptation rates $\dot{k}$. For humans, the distribution of ($\dot{\alpha}$,$\dot{L}$)-pairs is

elongated and oriented parallel to the $\gamma = 180°$ line. With increasing speed this distribution expands and shifts away from $\gamma = 180°$. By contrast, the avian distribution of $(\dot{\alpha},\dot{L})$-pairs is circularly clustered and does not enlarge with speed. Furthermore the avian $(\dot{\alpha},\dot{L})$-cluster is largely covered by the wedge-shaped area of predicted stability.

Figure 7 shows the grand means of the normalized maximum drop (NMD) as a function of angle of attack α_{TD} (subfigure (a)), leg rotation $\dot{\alpha}$ (subfigure (b)) and leg length change $\dot{L}$ (subfigure (c)) for different speeds. Compared to humans (green dots), birds (red triangles) run with flatter angles of attack and higher retraction speeds. Additionally, birds lengthen their legs before touching the ground, while humans shorten them. This combination of strategies results in a higher avian NMD, compared to the human NMD.

4. Discussion

This study investigated differences in leg kinematics and implied swing leg control strategies between human and avian bipedal running. The analysis of these swing leg control strategies using a simple spring mass model allowed the comparison of stability and robustness characteristics for human-like and bird-like running. Model based findings were compared with experimental data from humans and pheasants, exemplifying straight-legged versus bent-legged running postures. Stability, which is the system's ability to reduce a deviation in the CoM trajectory caused by a onetime perturbation, was estimated using limit cycle stability analysis (section 2.2). To evaluate the robustness, which is determined by the maximum perturbation the system can cope with, a new intuitive and easily accessible parameter, the NMD (section 2.3), was applied.

The bent posture of the bird-like leg provides an important advantage for swing leg control strategies in running. It possesses an increased ability for leg parameter adaptation, as it can be both lengthened and shortened in preparation for the TD. However, running with bent legs is also expected to reduce leg stiffness, require increased muscle forces to support body weight, and result in increased energy consumption (McMahon et al., 1987). As tissue strengths and specific muscle forces (force/area) are similar in animals of different size, the inevitable size-dependent adaptations relate to changes in skeletal form and muscle mechanics (Pearson and Misiaszek, 2001; Biewener, 1990). Therefore, due to limits to muscle and bone strength in large animals, only smaller and more lightweight animals run with crouched postures,

whereas larger species run more straight (Biewener, 1989). Taking birds as an example: small birds like the painted quail (*Excalfactoria*, $m \approx 0.05\,\mathrm{kg}$, $L_0 \approx 0.05\,\mathrm{m}$) walk and run very crouched, while tall birds such as the rhea (*Rhea*, $m \approx 20\,\mathrm{kg}$, $L_0 \approx 0.8\,\mathrm{m}$) have a rather straight leg posture (Gatesy and Biewener, 1991). In the following sections we want to further elucidate the advantages and disadvantages of crouched locomotion.

4.1. Swing phase

Leg kinematics of human and avian running differ significantly from each other and two distinct running strategies are observed (figure 5). Due to the straight posture of the human leg, most of the gait cycle the leg length is below $L = L_0$ (figure 5 (a) and (b)). As mentioned above, the contact phase of human running is slightly asymmetric, as the leg angle at TD is steeper than at TO. There also exists an asymmetry within the leg length (Cavagna, 2006). In heel-toe-running, the CoP moves during stance from heel to toe (Bullimore and Burn, 2006), and the lift of the heel causes a lengthening of the leg (Maykranz et al., 2009). However, to demonstrate leg kinematics during both phases stance and swing, we defined a hybrid leg between the CoM and the foot point, which neglects the effect of leg lengthening due to the influence of the foot.

The asymmetric shape of the human phase plots and the accentuated turning point, at which leg retraction is initiated (shortly before TD), suggest that the preparation of the ground contact is crucial. This could be due to the fact that, as humans touch the ground with a very extended leg posture, they have to retract and bend their legs shortly before TD to reduce the landing impacts and prevent their knees from damage. In contrast, the smooth and symmetric phase plots of avian running (figure 5 (c) and (d)) appear as the movements of a clock-driven pendulum.

4.2. Landing strategy

Ground speed matching (GSM) and the angle of approach γ indicate the magnitude and the direction of the foot's landing velocity vector and qualitatively estimate the impact a real leg would experience (section 2.1). Touching the ground with 100% GSM stands for a smooth and absolutely impact-free landing, while 0% GSM means that the foot moves with the same speed as the CoM. GSM < 0 indicates that the foot is actively pushed towards the ground and the resulting impact is enforced. $\gamma = 90°$ means that the foot approaches the ground perpendicular (i.e. the foot's velocity

vector has only a vertical component). Accordingly, $\gamma = 180°$ means that the foot approaches parallel to the ground (i.e. the foot's velocity vector has only a horizontal component).

As the human kinematic control parameters ($\dot{\alpha}$,$\dot{L}$) are distributed parallel and near to $\gamma = 180°$ (figure 6(a) and (b)), this suggests that humans avoid vertical impacts. They shorten their legs before TD (which is in accordance to the findings of Seyfarth et al. (2003)), and thus smooth their landing. In contrast, the avian ($\dot{\alpha}$,$\dot{L}$)-pairs are circularly clustered and more distributed (figure 6(c) and (d)). As birds lengthen their legs (which is in accordance to the findings of Daley et al. (2007)), they do not reduce the TD-impact so much and their feet hit the ground with almost the same speed as the CoM. However, with increasing running speed, both humans and birds reduce their landing-impacts by increasing the GSM (figure 4).

4.3. Stability

Within the kinematic control space ($\dot{\alpha}$,$\dot{L}$), figure 6 shows model predicted stable areas, which satisfy $|s| < 0.5$ (gray wedges), in comparison with experimental data (green dots and red triangles). When the stiffness adaptation rate $\dot{k}$ gets smaller, the stable area (gray wedge) shifts to the left within the kinematic parameter space, while when $\dot{k}$ gets larger, the wedge shifts to the right (exemplarily displayed in subfigure(b)).

As humans run with rather straight leg posture, their leg architecture does not allow for larger leg extension. Leg retraction, which is a potential strategy to stabilize running patterns (Seyfarth et al., 2003), is also limited, as leg retraction speed is restricted due to physiological limitations. Doke et al. (2005) showed that the force and work, required to swing the leg back and forth, sharply increase with the frequency of the movement, which might explain the fourfold increase in metabolic cost they observed. Therefore, to achieve running stability, humans might take advantage of the control strategies' redundancy and adapt their leg stiffness in anticipation of the ground contact (figure 6 (a) and (b)). For low speeds (figure 6 (a)), the distribution of experimental ($\dot{\alpha}$,$\dot{L}$)-points is mostly covered by the predicted stable area that corresponds to one stiffness adaptation rate, namely leg softening ($\dot{k} = -1.6k_{\mathrm{TD}}/T$). This quality changes with increasing running speed. Whereas for low speeds, the predicted stiffness adaptation rate $\dot{k}$ remains almost constant, for higher speeds the model suggest a variation of $\dot{k}$ to explore the entire kinematic control area (figure 6 (b), $\dot{k} = [0, 10.8]k_{\mathrm{TD}}/T$). With increasing running speed the predicted control strategy changes from

leg softening to leg stiffening (table 1). In contrast, for birds a constant $\dot{k}$ seems to be sufficient for properly selected kinematics control strategies ($\dot{\alpha}$,$\dot{L}$) (figure 6 (c) and (d)).

Previous studies on human running and hopping have shown that leg stiffness is not a constant parameter, but that it is adjusted when the properties of the surface change (Ferris et al., 1998; Moritz and Farley, 2006). Although the leg stiffness of humans and animals during level running does not even change much with speed (Farley et al., 1993), which is consistent to our findings (table 1 and 2, figure 4), our results predict that human leg stiffness is adjusted in anticipation of ground contact with a speed-dependent changing rate $\dot{k}$ (figure 4, table 3). However, this behavior would only be revealed experimentally through perturbations of the terrain height, and our findings might explain the results of recent studies: Grimmer et al. (2008) found that with increasing step height Δh the estimated leg stiffness of a human runner decreases ($k_{\text{Leg}} = 32.5\,\text{BW}/L_0$ for $\Delta h = 0$, $k_{\text{Leg}} = 23.7\,\text{BW}/L_0$ for $\Delta h = 15\,\text{cm}$, $v_x > 3.5\,\text{m/s}$). As an increase in step height results in a decrease in the flight time, this suggests that the human leg is stiffened during late flight phase This characteristic, namely leg stiffening in anticipation of ground contact for higher running speeds, corresponds to the results of our work (table 1). In contrast, Daley et al. (2007) could not find significant differences in avian leg stiffness when the birds (guinea fowl, *Numida meleagris*) ran over an unexpected perturbation (8.5 cm drop). This corresponds to our model prediction, suggesting that pheasants do not use a distinct stiffness adaptation as their predominant control strategy.

4.4. Robustness

The robustness of the simulated running solutions, in terms of the maximum drop height the system can cope with, was approximated by the NMD (figure 7), which is a function of the angle of attack α_{TD}, the leg rotation speed $\dot{\alpha}$ and the leg length change $\dot{L}$ (Appendix B). Compared to birds, the human combinations of steeper α_{TD}, lower $\dot{\alpha}$ and leg shortening ($\dot{L} < 0$) result in lower NMD values, whereas the influence of $\dot{L}$ predominates. Accordingly, the avian combinations of flatter α_{TD}, higher $\dot{\alpha}$ and leg lengthening ($\dot{L} < 0$) result in higher NMDs. However, compared to humans, birds retract their legs with much lower angular acceleration $\ddot{\alpha}$ (figure 4), and the actual drop height they can overcome might be even larger.

As Daley et al. (2006) showed by their drop down experiments, guinea fowls, (*Numida meleagris*) can easily negotiate drops of 8.5 cm, which corre-

sponds to 40% of their standing hip height L_0. If we transfer this into human scaling, this would mean to run over a drop of approximately 40 cm, which is hardly feasible. So far, we could only find literature concerning human running on uneven terrain with downward steps of 10 cm (Müller and Blickhan, 2010) and upward steps of 15 cm (Grimmer et al., 2008). Further perturbation studies are required to explicitly test these predictions for differing robustness of human versus avian locomotion.

5. Conclusion

This paper compared swing and landing behavior of avian and human running. Based on experimental data and spring mass simulations, predictions about stability, robustness and stiffness adaptation during swing phase were made.

- Birds lengthen their legs before TD ($\dot{L} > 0$), whereas humans shorten them ($\dot{L} < 0$).
- While model predictions suggest that birds might be able to stabilize their running pattern by using one constant stiffness adaptation rate $\dot{k}$, humans may have to adjust $\dot{k}$ on a larger scale to exploit the experimentally observed kinematic control space. With increasing running speed, the range of the predicted human $\dot{k}$ increases as well.
- Compared to humans, birds are more robust in terms of the normalized maximum drop NMD. Additionally, because birds retract their legs with much lower angular acceleration $\ddot{\alpha}$, the actual drop height they can overcome could be even larger.

We have shown that the applied control strategies are redundant in stabilizing the spring mass model. Therefore, a crouched leg posture does not necessarily enhance running stability. Nonetheless a crouched leg offers more adaptation possibilities, as it is capable of both leg lengthening and shortening. The question of whether a crouched leg posture enhances robustness can not be answered satisfactorily by solely taking the NMD as a basis, because this measure only estimates the upper bound for a drop perturbation, and ignores other limitations (e.g. size of the basin of attraction, peak force). Additionally, further investigation is required to extend the NMD concept

by taking angular acceleration $\ddot{\alpha}$ and leg length acceleration $\ddot{L}$ into account.

Further perturbation experiments on humans and animals in comparable conditions will be required to test many of the predictions resulting from our analysis here.

Appendix A - General description of limit cycle stability analysis

The system's state at the instant of apex is described by the state vector

$$\mathbf{S}_{\mathrm{i}} = (y_{\mathrm{A,i}}, v_{\mathrm{x,i}}), \tag{8}$$

with the index i enumerating the individual steps, $y_{\mathrm{A,i}}$ being the apex height and $v_{\mathrm{x,i}}$ the corresponding horizontal velocity. The Poincaré map is defined by

$$\mathbf{S}_{\mathrm{i+1}} = \mathbf{F}(\mathbf{S}_{\mathrm{i}}) \tag{9}$$

and a limit cycle trajectory corresponds to fixed points in each Poincaré map

$$\mathbf{S}^* = \mathbf{F}(\mathbf{S}^*). \tag{10}$$

To analyze the stability of the system in the neighborhood of the fixed point, the Poincaré map is linearized

$$\left[\mathbf{S}_{\mathrm{i+1}} - \mathbf{S}^*\right] \approx \mathbf{J}(\mathbf{S}^*)\left[\mathbf{S}_{\mathrm{i}} - \mathbf{S}^*\right] \tag{11}$$

and the eigenvalues λ_{i} of the Jacobian matrix $\mathbf{J}(\mathbf{S}^*)$ are evaluated. If the magnitude of all complex-valued eigenvalues is smaller than one $\|\lambda_{\mathrm{i}}\| < 1$, the limit cycle is stable (Dingwell and Kang, 2007; Guckenheimer and Holmes, 1983).

Assuming the system to be energy conserving, the apex height y_{A} and the horizontal velocity v_{x} are coupled by the energy $E = \frac{1}{2}\, m\, v_{\mathrm{x}}^2 + m\, g\, y_{\mathrm{A}}$. With this, the state vector can be reduced to

$$\mathbf{S}_{\mathrm{i}} = y_{\mathrm{A,i}} \tag{12}$$

and the Poincaré map (equation 9) becomes a one dimensional apex-return map

$$y_{\mathrm{i+1}} = \mathbf{F}(y_{\mathrm{i}}). \tag{13}$$

In this case, the Jacobian matrix $\mathbf{J}(\mathbf{S}^*) = \mathbf{J}(y^*)$ of the linearized Poincaré map $\left[y_{\mathrm{i+1}} - y^*\right] \approx \mathbf{J}(y^*)\left[y_{\mathrm{i}} - y^*\right]$ reduces to the one dimensional derivative

$$\mathbf{J}(y^*) = \left.\frac{dy_{\mathrm{i+1}}}{dy_{\mathrm{i}}}\right|_{y^*}, \tag{14}$$

which actually is the slope of the apex-return map (figure 3) in the neighborhood of the fixed point y^*.

Appendix B - Calculation of the normalized maximum drop (NMD)

The normalized maximum drop (NMD) (Daley and Usherwood, 2010) is a simple kinematic measure of the runner's ability to negotiate uneven terrain, which indicates the maximum drop $\Delta h_{\max}$ relative to the leg length L_0, the runner could overcome until the leg is vertically oriented ($\alpha = 90°$):

$$\text{NMD} = \frac{\Delta h_{\max}}{L_0}. \tag{15}$$

Here, the concept of the NMD is extended by allowing not only for constant leg retraction $\dot{\alpha}$, but also for constant leg length change $\dot{L}$ (figure 8).

Assuming the vertical position of the foot at the instant of nominal TD equals zero ($y_{\text{Foot,TD}} = 0$), the landing height of the CoM is

$$y_{\text{TD}} = L_{\text{TD}} \sin \alpha_{\text{TD}}. \tag{16}$$

Considering that the vertical component of the CoM velocity at apex equals zero ($\dot{y}_{\text{A}} = 0$), the vertical CoM speed at the instant of nominal TD results in

$$\dot{y}_{\text{TD}} = -g\, t_{\text{Fall}}. \tag{17}$$

The time Δt from the nominal TD until vertical leg orientation is reached is given by the remaining leg angle divided by leg retraction speed,

$$\Delta t = \frac{90° - \alpha_{\text{TD}}}{\dot{\alpha}}. \tag{18}$$

With this (equations 16 - 18), the CoM height of the maximum drop results in

$$y_{\text{Drop}} \;=\; y_{\text{TD}} + \dot{y}_{\text{TD}}\, \Delta t - \frac{g}{2}\,(\Delta t)^2, \tag{19}$$

and the corresponding vertical position of the foot and therefore the maximum drop yields

$$\Delta h_{\max} = y_{\text{Drop}} - \left(L_{\text{TD}} + \dot{L}\, \Delta t\right). \tag{20}$$

Acknowledgments

The authors thank J. Rummel and D. Maykranz for fruitful discussion and S. W. Lipfert for collecting and sharing the experimental data on human running. This work was supported by grants SE1042/1 and SE1042/7 of the DFG (German Research Foundation), grant RGY0062/2010 of the HFSP (Human Frontier Science Program), and a travel grant of the JEB (Journal of Experimental Biology).

Conflict of interest

The authors declare that there is no conflict of interest associated with this work.

References

Aerts, P., Van Damme, R., D'Aout, K., Van Hooydonck, B., 2003. Bipedalism in lizards: whole-body modelling reveals a possible spandrel. Philosophical Transactions of the Royal Society London B 358, 1525–1533.

Alexander, R. M., 1989. On the synchronization of breathing with running in wallabies (macropus spp.) and horses (equus caballus). Journal of Zoology 218 (1), 69–85.

Alexander, R. M., 2002. Tendon elasticity and muscle function. Comparative Biochemistry and Physiology A 133 (4), 1001–1011.

Alexander, R. M., 2004. Bipedal animals, and their differences from humans. Journal of Anatomy 204 (5), 321–30.

Biewener, A. A., 1989. Scaling body support in mammals: Limb posture and muscle mechanics. Science 245 (4913), 45–48.

Biewener, A. A., 1990. Biomechanics of mammalian terrestrial locomotion. Science 250, 1097–1103.

Blickhan, R., 1989. The spring-mass model for running and hopping. Journal of Biomechanics 22 (11-12), 1217–1227.

Blum, Y., Lipfert, S. W., Rummel, J., Seyfarth, A., 2010. Swing leg control in human running. Bioinspirations & Biomimetics 5 (2).

Blum, Y., Lipfert, S. W., Seyfarth, A., 2009. Effective leg stiffness in running. Journal of Biomechanics 42 (16), 2400–2405.

Bullimore, S. R., Burn, J. F., 2006. Consequences of forward translation of the point of force application for the mechanics of running. Journal of Theoretical Biology 238 (1), 211–219.

Cavagna, G. A., 2006. The landing-take-off asymmetry in human running. Journal of Experimental Biology 209 (20), 4051–4060.

Daley, M. A., Felix, G., Biewener, A. A., 2007. Running stability is enhanced by a proximo-distal gradient in joint neuromechanical control. Journal of Experimental Biology 210 (3), 383–394.

Daley, M. A., Usherwood, J. R., 2010. Two explanations for the compliant running paradox: Reduced work of bouncing viscera and increased stability in uneven terrain. Biology Letters 6 (3), 418–421.

Daley, M. A., Usherwood, J. R., Felix, G., Biewener, A. A., 2006. Running over rough terrain: guinea fowl maintain dynamic stability despite a large unexpected change in substrate height. Journal of Experimental Biology 209 (1), 171–187.

Dalleau, G., Belli, A., Viale, F., Lacour, J.-R., Bourdin, M., 2004. A simple method for field measurements of leg stiffness in hopping. International Journal of Sports Medicine 25 (3), 170–176.

De Wit, B., De Clercq, D., Aerts, P., 2000. Biomechanical analysis of the stance phase during barefoot and shod running. Journal of Biomechanics 33 (3), 269–278.

Dingwell, J. B., Kang, H. G., 2007. Differences between local and orbital dynamic stability during human walking. Journal of Biomechanical Engineering 129 (4), 586–593.

Djawdan, M., 1993. Locomotor performance of bipedal and quadrupedal heteromyid rodents. Functional Ecology 7 (2), 195–202.

Doke, J., Donelan, J. M., Kuo, A. D., 2005. Mechanics and energetics of swinging the human leg. Journal of Experimental Biology 208, 439–445.

Farley, C. T., Glasheen, J., McMahon, T. A., 1993. Running springs: speed and animal size. Journal of Experimental Biology 185, 71–86.

Ferris, D. P., Louie, M., Farley, C. T., 1998. Running in the real world: adjusting leg stiffness for different surfaces. Proceedings of the Royal Society B: Biological Sciences 265 (1400), 989–994.

Gatesy, S. M., Biewener, A. A., 1991. Bipedal locomotion: effects of speed, size and limb posture in birds and humans. Journal of Zoology 224 (1), 127–147.

Geyer, H., Seyfarth, A., Blickhan, R., 2005. Spring-mass running: simple approximate solution and application to gait stability. Journal of Theoretical Biology 232 (3), 315–328.

Geyer, H., Seyfarth, A., Blickhan, R., 2006. Compliant leg behaviour explains basic dynamics of walking and running. Proceedings of the Royal Society B: Biological Sciences 273 (1603), 2861–2867.

Grimmer, S., Ernst, M., Günther, M., Blickhan, R., 2008. Running on uneven ground: leg adjustment to vertical steps and self-stability. Journal of Experimental Biology 211 (18), 2989–3000.

Guckenheimer, J., Holmes, P., 1983. Nonlinear Oscillations, Dynamical Systems, and Bifurcations of Vector Fields. Applied Mathematical Sciences. Springer, New York.

Herr, H. M., McMahon, T. A., 2001. A galloping horse model. International Journal of Robotics Research 20 (1), 26–37.

Irschick, D. J., Jayne, B. C., 1999. Comparative three-dimensional kinematics of the hindlimb for high-speed bipedal and quadrupedal locomotion of lizards. Journal of Experimenta Biology 202 (9), 1047–1065.

Lipfert, S. W., 2010. Kinematic and Dynamic Similarities between Walking and Running. Verlag Dr. Kovac, Hamburg.

Maykranz, D., Grimmer, S., Lipfert, S. W., Seyfarth, A., 2009. Foot function in spring mass running. In: Autonome Mobile Systeme. Karlsruhe, Germany.

McGeer, T., 1993. Dynamics and control of bipedal locomotion. Journal of Theoretical Biology 163, 277–314.

McMahon, T. A., Cheng, G. C., 1990. The mechanics of running: how does stiffness couple with speed? Journal of Biomechanics 23 (1), 65–78.

McMahon, T. A., Valiant, G., Frederick, E. C., 1987. Groucho running. Journal of Applied Physiology 62 (6), 2326–2337.

Morin, J.-B., Dalleau, G., Kyrlinen, H., Jeannin, T., Belli, A., 2005. A simple method for measuring stiffness during running. Journal of Applied Biomechanics 21, 167–180.

Moritz, C. T., Farley, C. T., 2006. Human hoppers compensate for simultaneous changes in surface compression and damping. Journal of Biomechanics 39 (6), 1030–1038.

Müller, R., Blickhan, R., 2010. Running on uneven ground: Leg adjustments to altered ground level. Human Movement Science 29, 578–589.

Nelson, R. C., Dillman, C. J., Lagasse, P., Bickett, P., 1972. Biomechanics of overground versus treadmill running. Medicine and Science in Sports and Exercise 4 (4), 233–240.

Nigg, B. M., De Boer, R. W., Fisher, V., 1995. A kinematic comparison of overground and treadmill running. Medicine and Science in Sports and Exercise 27 (1), 98–105.

Pearson, K. G., Misiaszek, J. E., 2001. Locomotion. Encyclopedia of Life Sciences, http://www.els.net/[doi:10.1038/npg.els.0000163].

Rummel, J., Blum, Y., Maus, H. M., Rode, C., Seyfarth, A., 2010. Stable and robust walking with compliant legs. In: IEEE International Conference on Robotics and Automation. Anchorage, USA.

Schmitt, D., 2003. Insights into the evolution of human bipedalism from experimental studies of humans and other primates. Journal of Experimental Biology 206, 1437–1448.

Seyfarth, A., Geyer, H., Guenther, M., Blickhan, R., 2002. A movement criterion for running. Journal of Biomechanics 35 (5), 649–655.

Seyfarth, A., Geyer, H., Herr, H., 2003. Swing-leg retraction: a simple control model for stable running. Journal of Experimental Biology 206 (15), 2547–2555.

Strogatz, S. H., 1994. Nonlinear dynamics and chaos: With applications to physics, biology, chemistry, and engineering. Westview Press, Cambridge, Massachusetts.

Van Ingen Schenau, G. J., 1980. Some fundamental aspects of the biomechanics of overground versus treadmill locomotion. Medicine and Science in Sports and Exercise 12 (4), 257–261.

Windsor, D. E., Dagg, A. I., 2010. The gaits of the macropodinae (marsupialia). Journal of Zoology 163 (2), 165–175.

Table Legends

Table 1

Human running
Grand means and standard deviations of experimentally derived (upper section) and model based parameters (lower section) are listed for 7 subjects (1 female, 6 males, age $24 \pm 1\,\mathrm{yrs}$, body mass $m = 77 \pm 9\,\mathrm{kg}$, leg length $L_0 = 1.02 \pm 0.07\,\mathrm{m}$) at three different speeds.

Table 2

Avian running
Grand means and standard deviations of experimentally derived (upper section) and model based parameters (lower section) are listed for 5 adult male pheasants (*Phasianus colchicus*, body mass $m = 1.2 \pm 0.1\,\mathrm{kg}$, leg length $L_0 = 0.21 \pm 0.01\,\mathrm{m}$) at three different speeds.

Table 3

Regression analysis with respect to the Froude number
Statistics (slope, R^2, p-value) of the linear regression displayed in figure 4 are listed for humans and pheasants. Significant relationships (p-value ≤ 0.05) are indicated by an asterisk.

Tables

Table 1:

			Fr		
			0.42 ± 0.03	0.94 ± 0.06	1.66 ± 0.11
experimentally derived	v_{x}	[m/s]	2.06 ± 0.01	3.07 ± 0.01	4.07 ± 0.01
	T	[s]	0.78 ± 0.02	0.75 ± 0.02	0.70 ± 0.03
	$\alpha_{\mathrm{TD,exp}}$	[deg]	78.1 ± 1.0	73.8 ± 1.4	70.7 ± 1.9
	$\dot{\alpha}$	[deg/T]	35.6 ± 9.5	57.3 ± 13.2	82.2 ± 19.7
	$\ddot{\alpha}$	[deg/T^2]	1750 ± 160	2178 ± 139	2335 ± 186
	$\dot{L}$	[L_0/T]	-0.14 ± 0.06	-0.22 ± 0.07	-0.28 ± 0.08
	$\ddot{L}$	[L_0/T^2]	-7.4 ± 1.6	-11.6 ± 3.0	-13.4 ± 3.6
	k_{TD}	[BW/L_0]	21.5 ± 2.2	21.0 ± 3.4	21.3 ± 4.5
	GSM	[%]	34 ± 6	39 ± 7	43 ± 8
	γ	[deg]	160 ± 7	157 ± 6	152 ± 9
model based	$\alpha_{\mathrm{TD,sym}}$	[deg]	74.0 ± 1.4	70.1 ± 1.6	67.3 ± 2.0
	$\dot{k}$	[k_{TD}/T]	-1.6 ± 1.2	2.5 ± 1.3	5.4 ± 1.7
	NMD	[L_0]	0.48 ± 0.18	0.35 ± 0.12	0.25 ± 0.07

Table 2:

			Fr		
			2.32 ± 0.39	3.06 ± 0.19	3.68 ± 0.16
experimentally derived	v_{x}	[m/s]	2.22 ± 0.17	2.54 ± 0.08	2.77 ± 0.10
	T	[s]	0.35 ± 0.02	0.33 ± 0.02	0.31 ± 0.03
	$\alpha_{\mathrm{TD,exp}}$	[deg]	57.0 ± 4.3	57.6 ± 3.7	57.0 ± 1.6
	$\dot{\alpha}$	[deg/T]	93.9 ± 14.4	113.2 ± 20.0	132.4 ± 4.3
	$\ddot{\alpha}$	[deg/T^2]	1064 ± 223	971 ± 136	773 ± 222
	$\dot{L}$	[L_0/T]	0.95 ± 0.85	0.75 ± 0.64	0.49 ± 0.50
	$\ddot{L}$	[L_0/T^2]	-34.3 ± 6.3	-30.1 ± 3.8	-22.5 ± 2.6
	k_{TD}	[BW/L_0]	8.8 ± 1.7	9.8 ± 1.8	10.1 ± 1.2
	GSM	[%]	2 ± 19	8 ± 13	16 ± 10
	γ	[deg]	145 ± 9	143 ± 7	140 ± 2
model based	$\alpha_{\mathrm{TD,sym}}$	[deg]	52.5 ± 5.1	51.9 ± 4.2	51.5 ± 2.8
	$\dot{k}$	[k_{TD}/T]	0.3 ± 3.3	1.1 ± 2.3	2.6 ± 1.7
	NMD	[L_0]	0.99 ± 0.34	0.76 ± 0.30	0.55 ± 0.11

Table 3:

			Humans				Pheasants			
			slope	R^2	p-value		slope	R^2	p-value	
experimental	α_{TD}	[deg]	−6.0	0.84	< 0.001	*	−0.7	0.02	0.700	
	$\dot{\alpha}$	[deg/T]	39.4	0.74	< 0.001	*	25.0	0.48	0.018	*
	$\ddot{\alpha}$	[deg/T^2]	434.9	0.59	< 0.001	*	−127.9	0.13	0.271	
	$\dot{L}$	[L_0/T]	−0.1	0.45	0.001	*	−0.6	0.27	0.100	
	$\ddot{L}$	[L_0/T^2]	−4.5	0.40	0.002	*	8.2	0.60	0.005	*
	k_{TD}	[BW/L_0]	−0.6	0.01	0.599		0.7	0.06	0.479	
	GSM	[%]	7.6	0.28	0.014	*	15.4	0.42	0.030	*
	γ	[deg]	−6.4	0.20	0.045	*	−1.7	0.02	0.646	
model	$\dot{k}$	[k_{TD}/T]	5.7	0.84	< 0.001	*	2.9	0.45	0.023	*
	NMD	[L_0]	−0.2	0.38	0.003	*	−0.3	0.39	0.041	*

Figure Legends

Figure 1

Spring mass running

One step in spring mass running is defined by two subsequent apices. A point mass m (representing the body mass) is supported by a translational spring with rest length L_0, stiffness k_{TD} and angle of attack α_{TD}. Swing leg control strategies are: a) leg rotation $\dot{\alpha}$, b) leg length change $\dot{L}$ and c) stiffness adaptation of the leg spring $\dot{k}$.

Figure 2

Landing strategy

The adaptation rates $\dot{\alpha}$ and $\dot{L}$ of the kinematic parameters leg angle and leg length affect the magnitude v_{Foot} and the direction (indicated by the angle of approach γ) of the foot's landing velocity vector $\mathbf{v}_{\text{Foot}}$.

Figure 3

Apex-return map

In the return map $y_{i+1}(y_i)$, intersections with the diagonal $y_i = y_{i+1}$ denote fixed points y^*. In this example, the lower fixed point is stable ($s = -0.04$), the upper one unstable ($s = 1.60$).

Figure 4

Leg parameters

Mean values of experimentally derived and model based parameters for human (green dots) and avian (red triangles) running are plotted over speed (indicated as Froude number).

Figure 5

Phase plots

Experimentally observed kinematic leg parameters, leg angle α and leg length L, for human (subfigure (a) and (b)) and avian (subfigure (c) and (d)) running cycles are plotted against each other. The grand means of the trajectories are highlighted in green (human) and red (avian), respectively. The markers indicate touch down (TD), take off (TO) and TD and TO of the contralateral leg (TDc and TOc).

Figure 6

Running stability

Swing leg control, stability and foot landing strategy are shown for selected periodic solutions of spring mass running. Stable areas ($|s| < 0.5$) of the spring mass model, corresponding to selected stiffness adaptation rates $\dot{k}$, are indicated by the gray wedges. The relative foot point velocity (100% and 0% GSM are illustrated in blue) and the foot point's angle of approach γ (black lines) describe the foot landing strategy. The experimentally observed individual swing leg characteristics for human (green dots) and avian (red triangles) running at different speeds are shown, with the stable area matching the mean swing leg characteristics (black circle), assuming super-stable behavior ($s = 0.5$). ($\dot{\alpha} < 0$: leg protraction, $\dot{\alpha} > 0$: leg retraction, $\dot{L} < 0$: leg shortening, $\dot{L} > 0$: leg lengthening, $\dot{k} < 0$: leg softening, $\dot{k} > 0$: leg stiffening)

Figure 7

Normalized maximum drop (NMD)

The NMD's grand mean for human (green dots) and avian (red triangles) running is illustrated as a function of a) the angle of attack α_{TD}, (b) the leg rotation speed $\dot{\alpha}$ and c) the leg length change $\dot{L}$. The speeds correspond to the values listed in table 1 and 2.

Figures

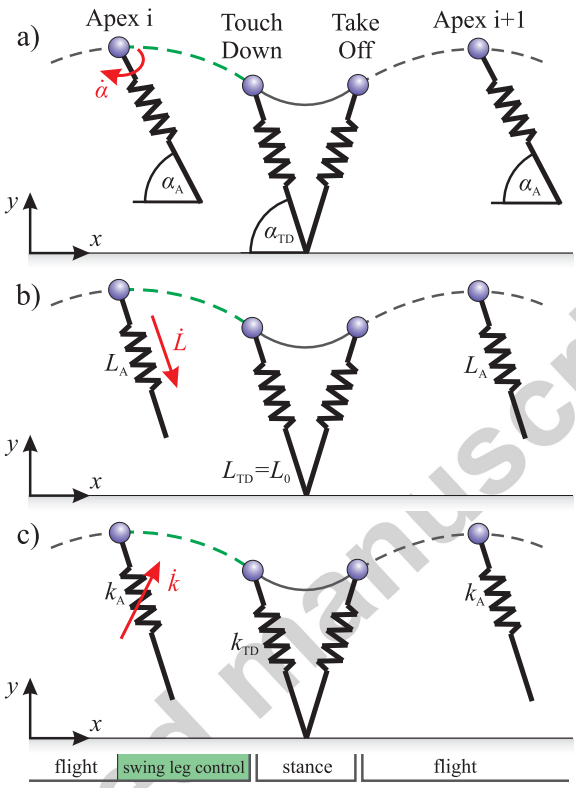

Figure 1:

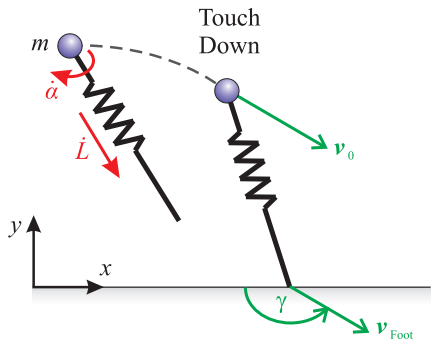

Figure 2:

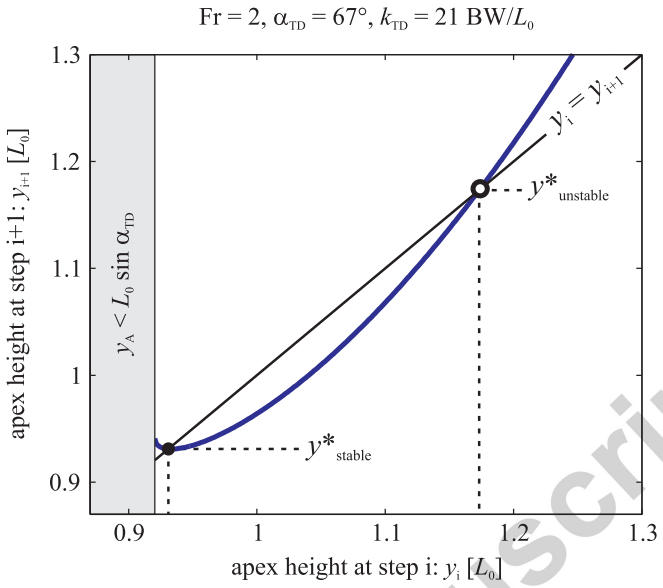

Figure 3:

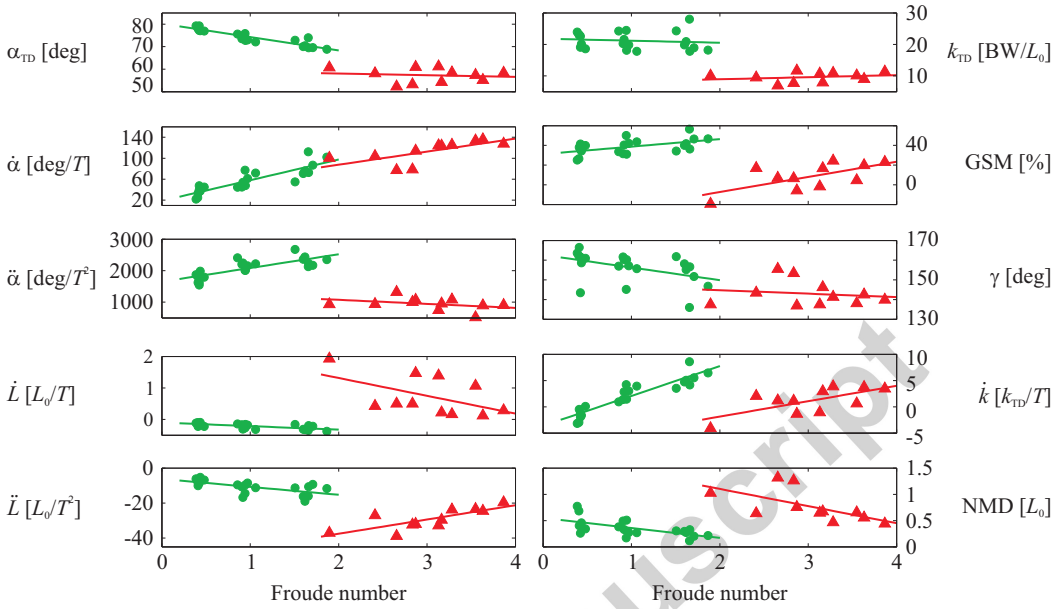

Figure 4:

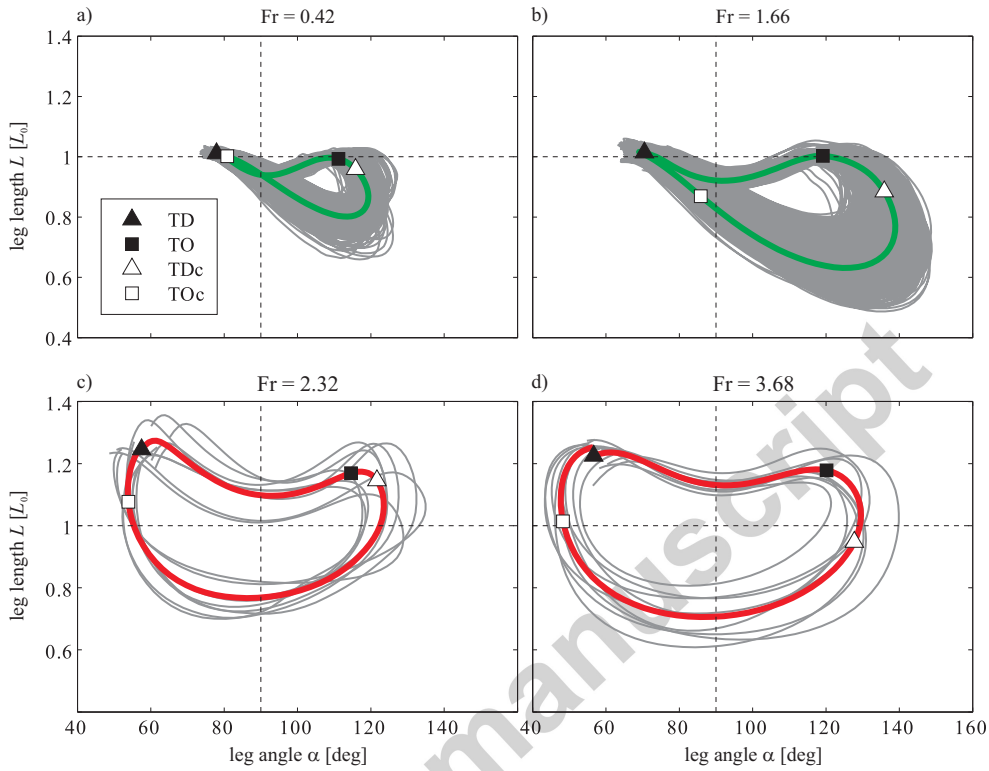

Figure 5:

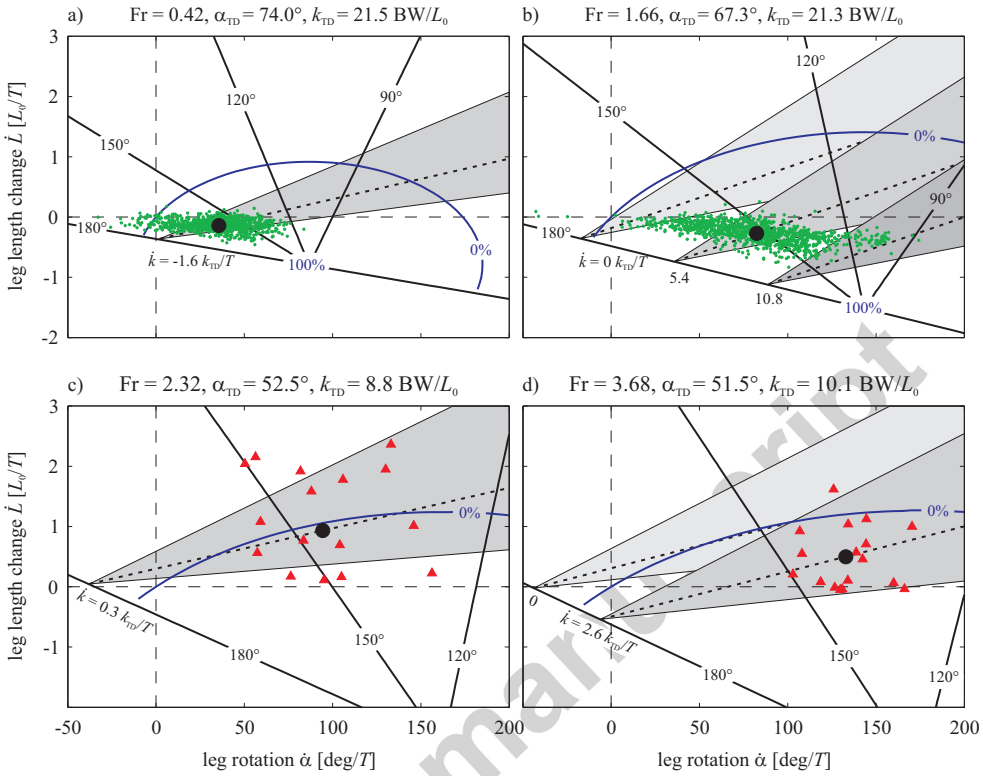

Figure 6:

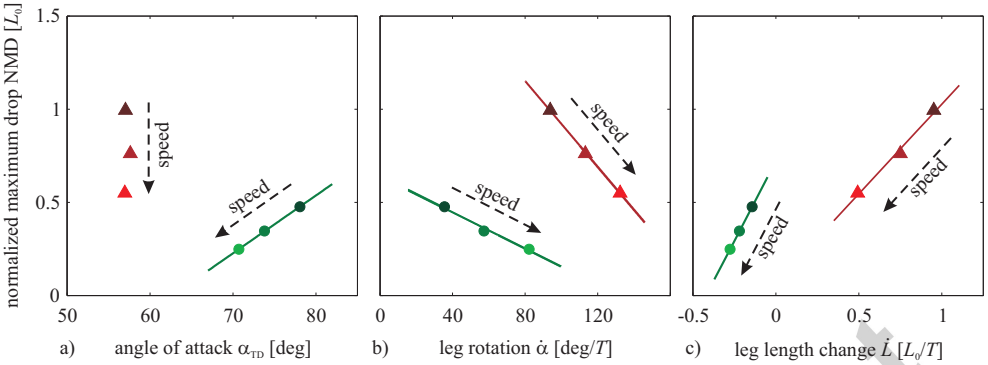

Figure 7:

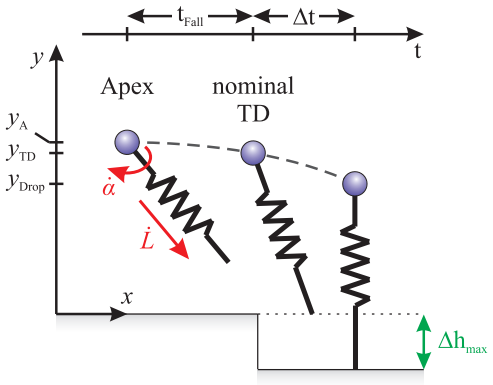

Figure 8:

Highlights

- We compared swing and landing behavior of avian and human running
- Based on experimental data and spring mass simulations, predictions about stability, robustness and stiffness adaptation during swing phase were made
- The model suggests that birds might be able to stabilize running by applying one constant stiffness adaptation rate
- Humans may have to adjust their leg stiffness on a larger scale
- Compared to humans, birds are more robust in terms of the maximum drop they can cope with